U.Porto Journal of Engineering, 10:1 (2024) 45-58
ISSN 2183-6493
DOI: 10.24840/2183-6493_0010-001_002060

Received: 16 February, 2023
Accepted: 24 January, 2024
Published: 6 February, 2024

Effect of Aging Heat Treatment in an Al-4008 Produced by Liquid Metal Printing

C. M. Ladeiro
Department of Metallurgical and Materials Engineering, Faculdade de Engenharia, Universidade do Porto, Rua Dr. Roberto Frias, 4200-465 PORTO, Portugal (up201806112@fe.up.pt) ORCID 0009-0003-8587-2309

F. L. Nunes
Department of Metallurgical and Materials Engineering, Faculdade de Engenharia, Universidade do Porto, Rua Dr. Roberto Frias, 4200-465 PORTO, Portugal (up201806193@fe.up.pt) ORCID 0009-0000-0988-4285

M. M. Trindade
Department of Metallurgical and Materials Engineering, Faculdade de Engenharia, Universidade do Porto, Rua Dr. Roberto Frias, 4200-465 PORTO, Portugal (up201806438@fe.up.pt) ORCID 0009-0008-1397-5321

J. M. Costa
Department of Metallurgical and Materials Engineering, Faculdade de Engenharia, Universidade do Porto and LAETA/INEGI - Institute of Science and Innovation in Mechanical and Industrial Engineering, Rua Dr. Roberto Frias, 4200-465 PORTO, Portugal (jose.costa@fe.up.pt) ORCID 0000-0002-1714-4671

Author Keywords

Liquid Metal Printing, Additive Manufacturing, Aluminum 4008, Heat Treatment.

Type: Research Article

Open Access
Peer Reviewed

Abstract

In today's world, additive manufacturing (AM) is one of the most popular technologies and has the potential to revolutionize the manufacturing industry. As one of the most recent advances in this industry, liquid metal printing has a growing value in the engineering field. This study aims to evaluate the effect of two heat treatment conditions in an Al-4008 alloy produced by this technique in the microstructure and mechanical properties. It was concluded that the heat treatment (HT) enhances the Si particle coalescence and Fe-rich intermetallic compound precipitation, increasing the sample hardness significantly (50%). Density analysis showed a slight porosity decrease with HT. Tensile tests indicated heat-treated, same-directionally pulled samples exhibited brittleness compared to as-printed ones, while HT increased both yield strength (245 MPa) and ultimate tensile strength (294 MPa).

1. Introduction

The numerous applications in the contemporary industry of aluminum and its abundance in the Earth's crust has promoted the increase of the outputs of this material by more than 50% globally during the past 10 years. Aluminum is used mostly for housings, engine components, production tools, and molds in several industries, such as automotive and automation since these types of industries may benefit from aluminum's properties. Among these, it is possible to remark its low weight, high strength, various post-processing possibilities, the creation of an adherent surface oxide deposit promoting a higher corrosion resistance, high laser reflectivity, high thermal conductivity, and thermal expansion (Lumley; Melamed et al. 2021). Additive manufacturing (AM) widely refers to innovative technologies that enable everyone, from major corporations to individual consumers, to print three-dimensional (3D) and four-dimensional (4D) products. The term "4D printing" refers to 3D printing part that changed

itself to another structure, throughout time. The application of AM to aluminum alloys used to be more limited, partially because these alloys, unlike others, are well suited for low-cost production using traditional manufacturing processes, such as die casting and machining. Additionally, several of their innate physical characteristics appeared to restrict AM's wider applicability to these alloys (Lumley; Kamara and Faggiani; Ansell 2021; Reddy and Devi 2018). A new and expanding family of related printing technologies called liquid metal printing is used to create full or almost free-standing metal objects and it belongs to the AM method family known as material jetting (Ansell 2021). The main difference between these two techniques is that, in material jetting, there is a deposition of both the material that it is intended to print, and the support material. In the case of liquid metal printing, only the build material is deposited (Gülcan, Günaydın and Tamer 2021).

Since the jetting technologies are based on widely used inkjet printers and the volume of the liquid metal is not a limiting factor, liquid metal jetting (LMJ) is more scalable than powder-based or wire-based AM techniques. The capacity to melt the material prior to jetting is the only prerequisite for LMJ, as opposed to melting powder either in situ or during post-processing. This results in an expansion of the spectrum of printable metal alloys. The drawbacks of beam-based metal AM may be solved by liquid metal printing, particularly in terms of reducing temperature-related problems such as hot cracking. The most recent International Organization for Standardization/ASTM International (ISO/ASTM) standard on AM nomenclature defines material jetting as a “process in which droplets of build material are selectively deposited” onto a substrate, being similar to material extrusion because nozzles or orifices are also used to regulate the flow of the material (ISO/ASTM 2015; Ansell 2021; American Institute of and Astronautics). Figure 1 shows the scheme of liquid metal printing process (Flow-3D 2022). In this case, an electrically pulsed coil, encircling the ejection chamber, melting the metal due to Joule effect, creates a temporary magnetic field, that permeates the liquid metal and causes a closed loop transient electric field inside of it, which will promote a magnetohydrodynamic Lorentz force density inside the chamber. This induces a pressure that will force the liquid metal droplet into the substrate, where it solidifies to form extended solid structures (Flow-3D 2022).

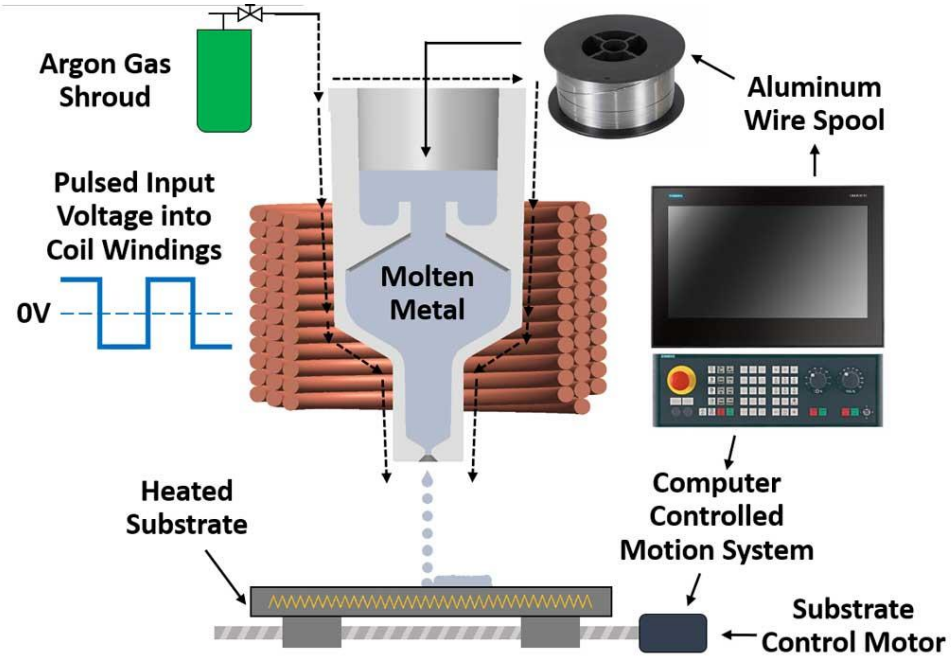

Figure 1: Scheme of liquid metal printing process.

To print liquid metal, there are two distinct printing processes that are based on commercial inkjet printing technology: continuous printing and drop-on-demand (DOD). This two differ on the fact that, in the first one, the drops of metal are continuously being deposed in the support metal, whereas in the DOD, the metal is only deposited when needed. The capacity to fabricate complex parts using printers and CAD/CAM software typically exceeds classic casting processes. This process includes jetting liquid metal into a solid freeform structure while following a computer design. Several of the current AM development targets may be accomplished through this type of manufacturing procedure. In contrast to powder-bed techniques, like selective laser sintering/melting, liquid metal printing could make it possible to print non-weldable metals and its alloys (Ansell 2021; American Institute of and Astronautics). Furthermore, it is not necessary to use molds or masks for printing liquid metal designs, resulting on a quicker manufacturing cycle of the printing technique (Chen et al. 2022).

Liquid metal exhibits a naturally occurring, atomically thin oxide coating on its surface when exposed to atmospheric conditions. This type of metal oxide may attach effectively to other oxides (such as silicon dioxide and silicon), forming a oxide coating that sticks securely to the substrate surface according to Van Der Waals force. (Huang et al. 2021; Li et al. 2021).

Xerox ElemX^{TM} Liquid Metal Printer offers lower cycle times since there is no powder removal, debinding, or sintering. Additionally, known material attributes are equivalent to or superior than input material, and only minimal heat and argon-related safety precautions are needed (Xerox 2021). The equipment uses a 4008 aluminum alloy (composition in Table 1), equivalent to casting alloy A356, available as a continuous solid metal wire, and commonly used as wire feedstock for welding process (MIG). For reference, Al-Si phase diagram is presented in Figure 2 (Biswas, Patra and Mondal 2020).

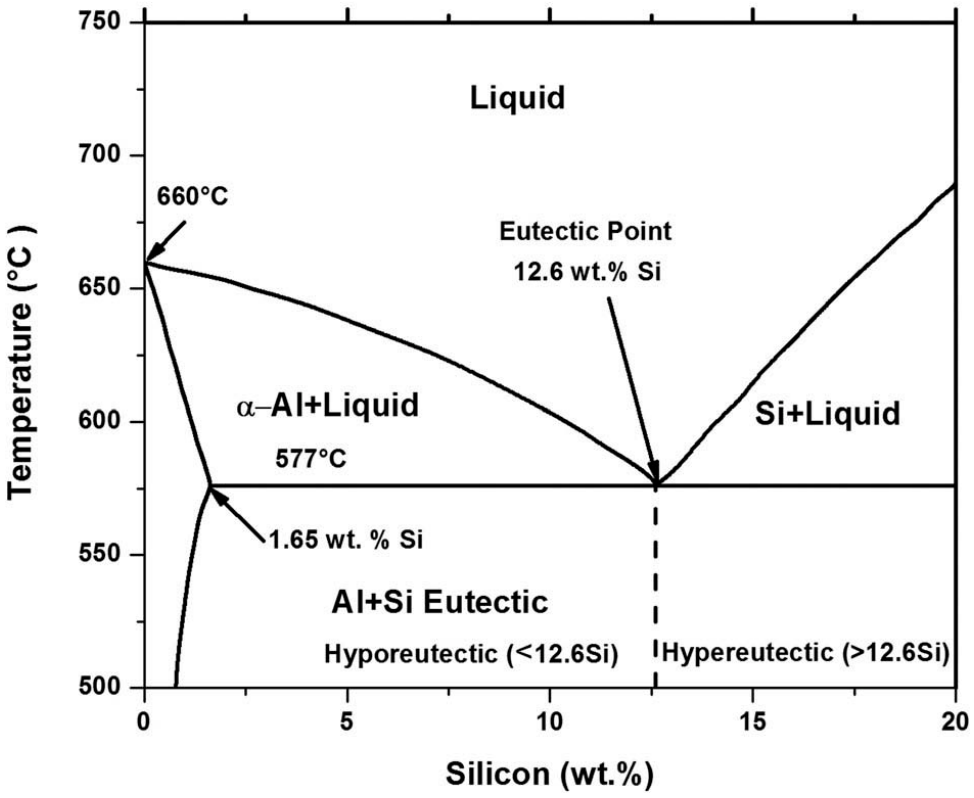

Figure 2: Al-Si phase diagram.

2. Materials and Methods

2.1. Materials

Two small parts made of 4008 aluminum alloy, supplied by Xerox (Headquarters Norwalk, Connecticut, United States), additively manufactured by Xerox ElemX™ Liquid Metal Printer, were used in this study. Table 1 presents the chemical composition of Al-4008 samples.

Alloy	Chemical Composition (% wt)							
	Si	Fe	Cu	Mn	Mg	Zn	Ti	Al
Al-4008	7	0.08	<0.01	<0.01	0.40	<0.01	0.08	Bal.

Table 1: Chemical composition of Al-4008 samples.

2.2. Heat Treatment

The parts were cut using a cut-off machine with cooling to prevent substrate and cladding overheating, to get five small cubes and four parallelepipeds to perform the tensile tests. Table 2 presents the conditions for each sample. (two for each direction: A, C - perpendicular to the deposition direction; B, D - parallel to the deposition direction).

Sample	Deposition Direction	HT
A1	Parallel	T6 (i)
A2		T6 (ii)
B1	Perpendicular	T6 (i)
B2		T6 (ii)
C1	Parallel	T6 (i)
C2		T6 (ii)
D1	Perpendicular	T6 (i)
D2		T6 (ii)

Table 2: Conditions of the studied samples.

Four cubes and two parallelepipeds were subjected to the T6 heat treatment, which was done with the same conditions, varying only the medium in aging treatment in a polymer bath (Huber CC304) due to capabilities to apply a uniform heating, in a reduced oxygen atmosphere. The controlled heating and cooling cycles in a polymer bath furnace can help minimize distortion and internal stresses in the material, resulting in improved dimensional stability and mechanical performance. Both procedures are exposed in Table 3.

Heat Treatment	Solutions Temperature/Time	Quench Medium	Aging Temperature/Time	Final Cooling
T6 (i)	538 °C for 4h	Water	155 °C for 3h (muffle furnace)	Air
T6 (ii)			155 °C for 3h (polymer bath)	

Table 3: Heat treatment procedures.

2.3. Microstructural and mechanical characterization

The analysis of the samples should be done in the perpendicular plane to the direction of the built plate (Z direction), as shown in Figure 3. For microstructural and mechanical characterization, after the heat treatment (HT), the samples were set in epoxy resin and polished down to 1 µm diamond suspension. For a better surface finish and to remove polishing-induced plastic deformation, a second polishing step using 0,06 µm silica colloidal suspension was conducted.

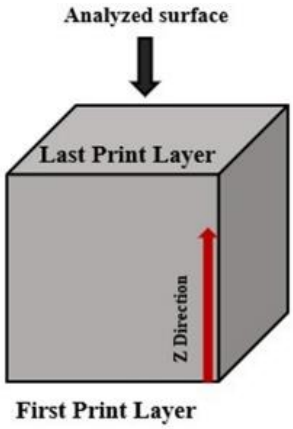

Figure 3: Direction deposition according to the built plate.

The microstructural and chemical analysis were performed, respectively by an optical microscope (OM) Leica DVM6, and a scanning electron microscope (SEM) FEI Quanta 400 FEG ESEM with energy dispersive X-ray spectroscopy (EDS) EDAX Genesis X4M. To reveal the microstructure, a NaOH solution (mixture of 5 g of NaOH and 100 mL of distilled water) was used as chemical etchant. Furthermore, it was also analyzed the density through ImageJ software, however, it was not considered enough fields, per condition of treatment, to create a statistical study.

The microhardness test was conducted using a microindenter Struers Duramin, set to Vickers Hardness, applying a load of 100 gf (HV 0.1) and a dwell time of 15 seconds. Each sample was subjected to five measurements.

Concerning to the tensile tests it was used a Instron 5900R, firstly, the test specimens were machined according to the geometry and dimensions shown in Figure 4 and with a thickness of 3,30 mm. Notice that two samples were machined for four different conditions: two with HT-T6 (i) in the perpendicular direction of metal deposition (A1, A2) and two in the parallel direction (B1, B2); two as-printed in the perpendicular direction of metal deposition (C1, C2) and two in the parallel direction (D1, D2). Subsequently, the test took place, at room temperature, on an electromechanical uniaxial testing system applying a load of 5kN and with a crosshead speed of 1,25 mm/min. Also, the extensometer gage length used was 25 mm and the acquisition rate was 10 Hz.

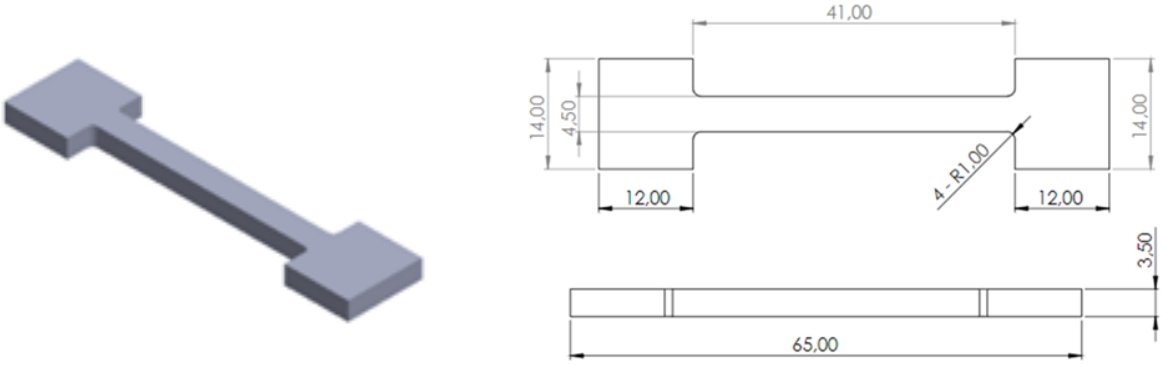

Figure 4: Uniaxial tensile test specimen geometry and dimensions (in mm).

3. Discussion

3.1. Microstructure

Considering Figure 5, the microstructural variation of the HT samples comparing to the as-printed sample is remarkable. Figure 5a presents a structure consisting of α-Al, Si eutectic, uniformly distributed in the matrix, as predicted from phase diagram. However, after aging,

the Si intermetallic compounds coalesce and growth. Additionally, Fe-rich intermetallic compounds, in the form of fine and elongated needles, are evident in Figure 5b and Figure 5c. Although the aging procedure had been done in different environments, the microstructure of the samples did not change significantly.

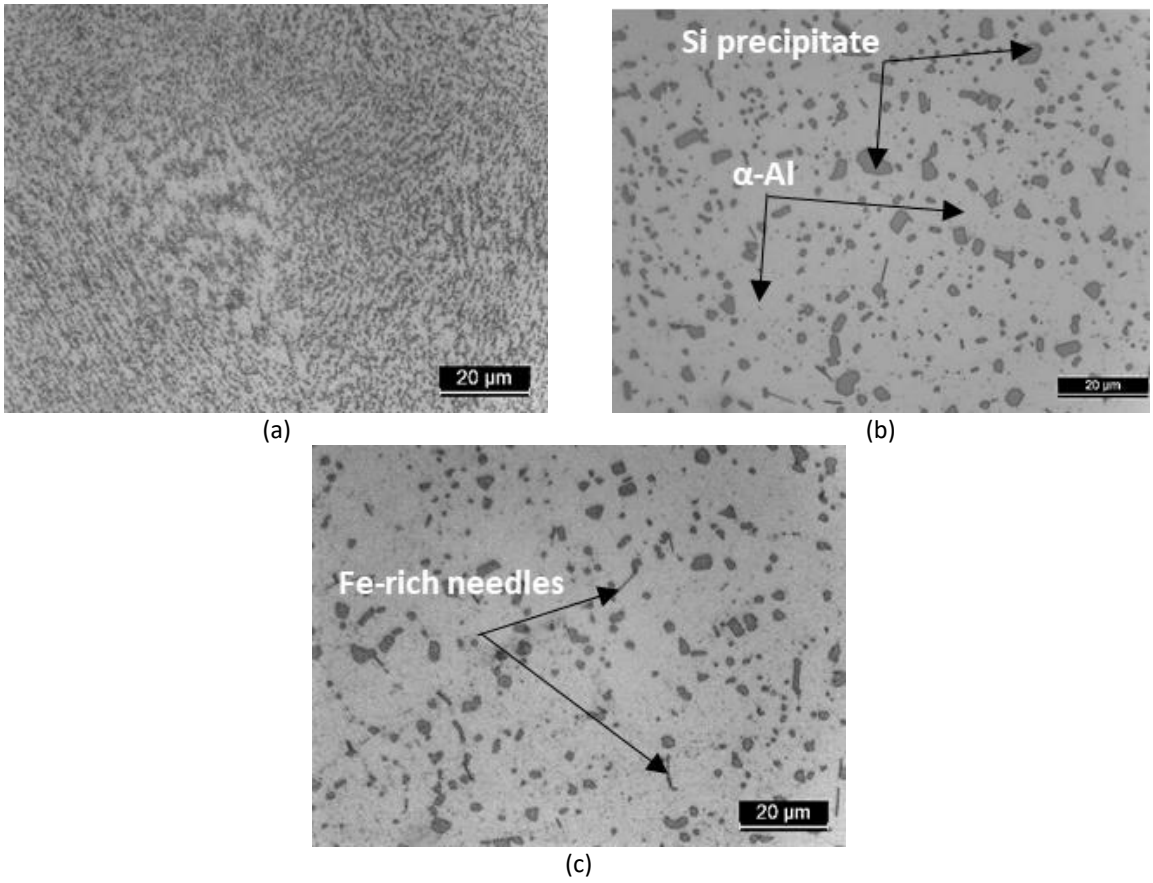

Figure 5: Microstructure of the sample: A- as-printed; B- with HT-T6 (i) and C- with HT-T6 (ii).

SEM emphasized the HT-T6 (i) sample morphology, as well as the chemical composition, which is shown in Table 4, of the zones identified in Figure 6a. The SEM-EDS evaluation allowed to verify, in this way, which were the constituent compositions of the structure of the HT samples. Thus, it turns out that the samples are composed of an Al matrix (Z1) (Figure 6b), $AlSi_2$ (Z2) compounds (Figure 6c) and Fe-rich compounds, namely, β-Al_5FeSi (Z3) (Figure 6d). Notice that the Al-Si phase diagram do not predict the formation of the compound identified by Z2, but only the formation of Al and eutectic constituent, due to inaccuracy of EDS method (Xerox 2021; Chao et al. 2018; Domfang Ngnekou et al. 2017; Biswas, Patra and Mondal 2020). However, the SEM- EDS analysis revealed the presence of the compound mentioned before ($AlSi_2$).

Phases	Chemical Composition (% wt)							
	Si	Fe	Cu	Mn	Mg	Zn	Ti	Al
Z1	1.32	-	-	-	1.0	-	-	97.67
Z2	60.8	-	-	-	0.38	-	-	38.83
Z3	11.39	6.9	-	-	-	-	-	81.7

Table 4: Phase chemical analysis obtained by SEM-EDS.

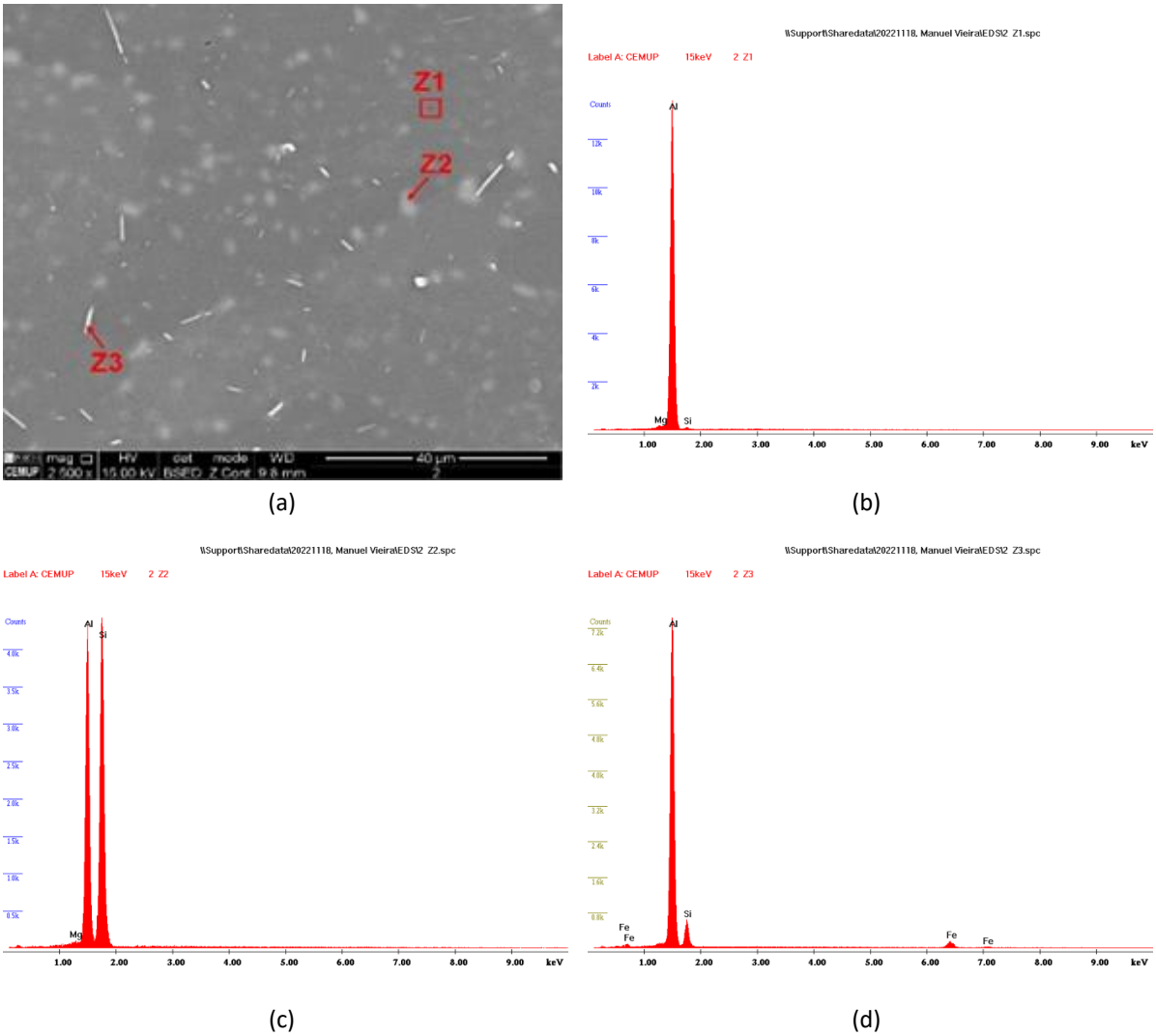

Figure 6: SEM image showing the EDS surface analysis structures for the Al-4008 (a), and EDS chemical analysis for Z1 (b), Z2 (c), and Z3 (d).

Furthermore, in some regions of the sample there is lack of coalescence (Figure 7) resulting of the liquid metal printing process. The void assumes the droplet geometry, acquiring a rounded morphology.

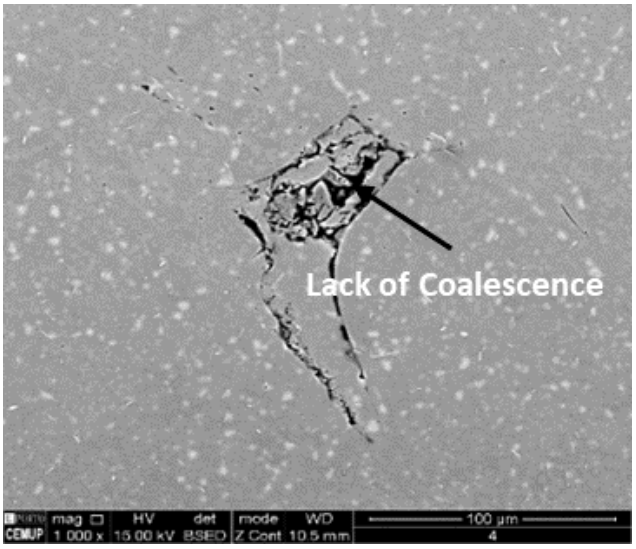

Figure 7: Lack of coalescence in sample.

Optical microscope also highlighted some droplets in the structure, as shown in Figure 8, which is noteworthy by larger intermetallic compounds in the boundary. However, the presence of this structure is not uniform across the sample. The formation of this structure may have occurred due to the higher surface solidification rate of the droplet, and the formation of a thin oxide layer in the surface, during the LMJ process, as consequence of environmental conditions, and in this way, the drop had higher surface tension, lower adhesion to the substrate and higher surface energy in the droplet boundary.

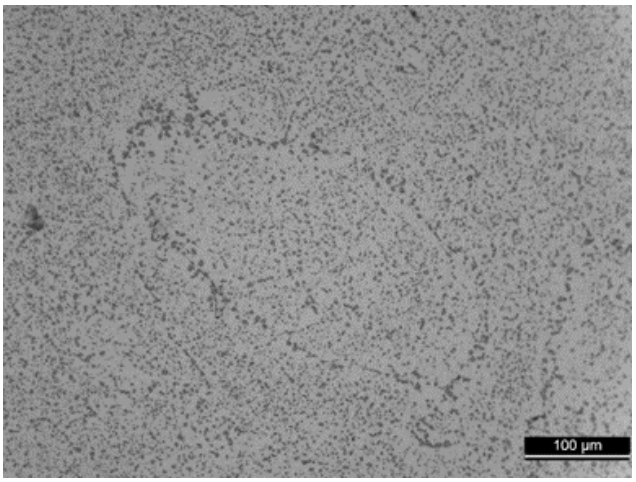

Figure 8: Droplet boundary in the microstructure.

3.2. Microhardness

The Table 5 and the graph Figure 9 show, respectively, the results of the five Vickers microhardness indentations and their variation according to the treatment the samples were submitted to.

As expected, the microhardness increases with application of the HT-T6, with a value of nearly 50 %. This growth occurs due to the heat treatment which has promoted the precipitation and coalescence of Si compounds ($AlSi_2$), and due to an unexpected phenomenon found where exists the formation of thin and elongated needles of Fe- rich intermetallic compounds (β-Al_5FeSi), which are hard and brittle.

The average value obtained from the five identifications is within the expected value for this material in both as-printed and HT condition. However, the measurements might have been made near to porosities and droplet's boundaries inducing some variations, represented by the standard deviations, and in this case were not which are not very significant (Corporation, 2022).

Sample	Indentation					Mean
	1	2	3	4	5	
As-printed	54	61	57	56	59	57 ± 2
T6 (i)	105	116	98	105	107	108 ± 5
	105	112	105	114	112	
T6 (ii)	112	115	117	114	112	112 ± 3
	112	112	110	105	107	

Table 5: Hardness obtained in each five indentations and their average per heat treatment.

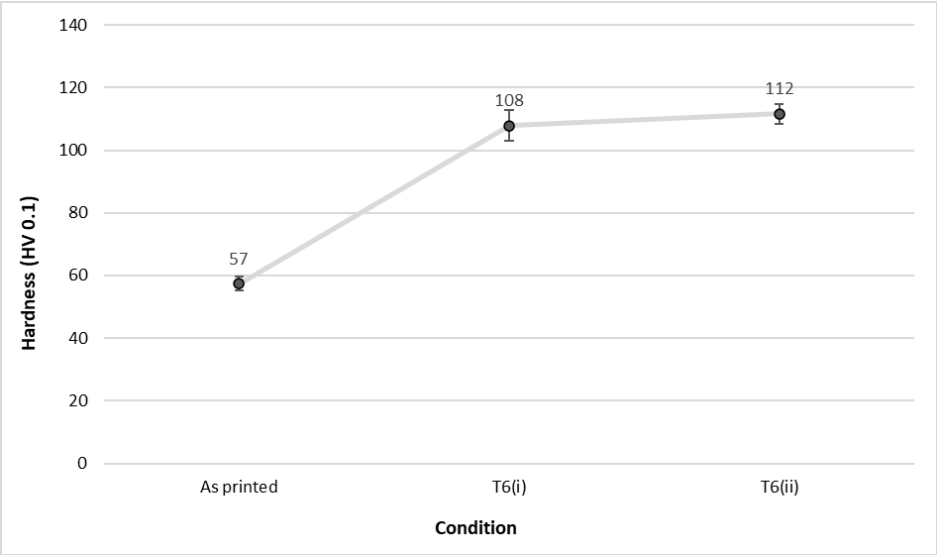

Figure 9: Evolution of the microhardness with the type of treatment that the samples were subjected.

Comparing the samples that had different aging treatments (T6 (i) and T6 (ii)), there is a slight increase of the hardness within the use of polymer bath, but since this variation it is not considerable, it may be concluded that the microhardness is not significantly changed using two distinct aging mediums, since the heat treatment temperature and time, in both cases, are the same, although the existence of a lower temperature control in the muffle furnace. Furthermore, the procedure was made in the exact same way, with a minimum delay between each stage, promoting the lowest possible variation in the measurements done.

3.3. Density

The use of liquid metal jetting process in this material promotes two different types of void discontinuities, including gas porosity, caused by hydrogen dissolved in liquid aluminum, and voids due to a lack of coalescence, which happens when crevices in a row or layer are partially filled by droplets being deposited alongside or on top of the deposited material.

Using optical microscope and ImageJ software, it was possible to determine the percentage of porosity for each sample, presented in Table 6 and Figure 10a), and to calculate the density (Figure 10b), which varies between 98,9% and 99,5%, as expected (Xerox 2021). For this purpose, it was used the broadest field possible (magnification of 5x) and particular attention was paid to the fact that silicon particles could be mistakenly categorized as voids. Notice that, since there are not enough fields analyzed, the results are not totally representative of the samples' density.

As a result, it was noticed that the application of HT-T6 decreases, slightly, the percentage of porosity (Table 6). This happens since, during the solution treatment at temperatures near to the melting point, followed by quench, a high thermal gradient is promoted, resulting in shrinkage, that will slightly reduce the amount of porosity present in the samples. The porosity constitutes places of stress concentrations, propitiating the propagation of cracks in the material.

Samples		Porosity (%)	Mean (%)	Density (%)
As-printed		1.059	1.059	98.9
T6 (i)	**1**	0.260	0456	99.5
	2	0.670		
T6 (ii)	**3**	0.123	0767	99.2
	4	1.410		

Table 6: Percentage of porosity and density for each sample.

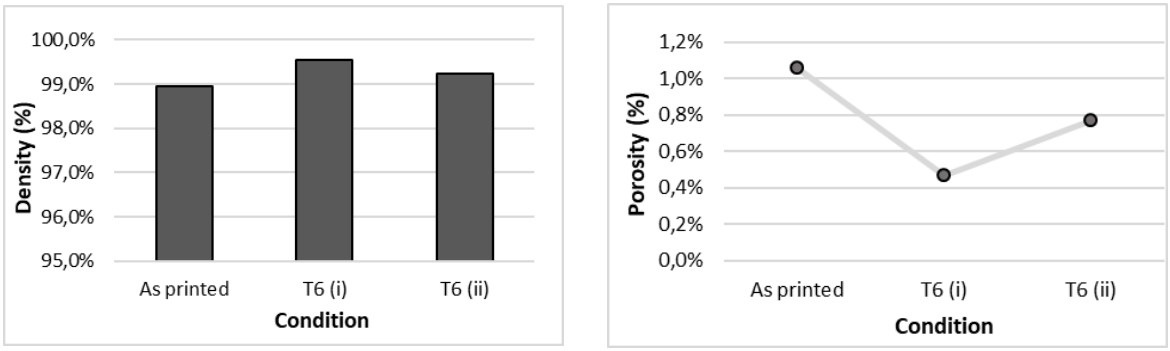

(a) (b)

Figure 10: Densification percentage for each HT condition (a) and percentage of porosity (b).

Figure 11 shows examples of voids analyzed by ImageJ, which were considered when making the measurements. It is possible to affirm that these discontinuities normally are found in the middle of a droplet, but they also can be seen, occasionally, near droplet or layer boundaries.

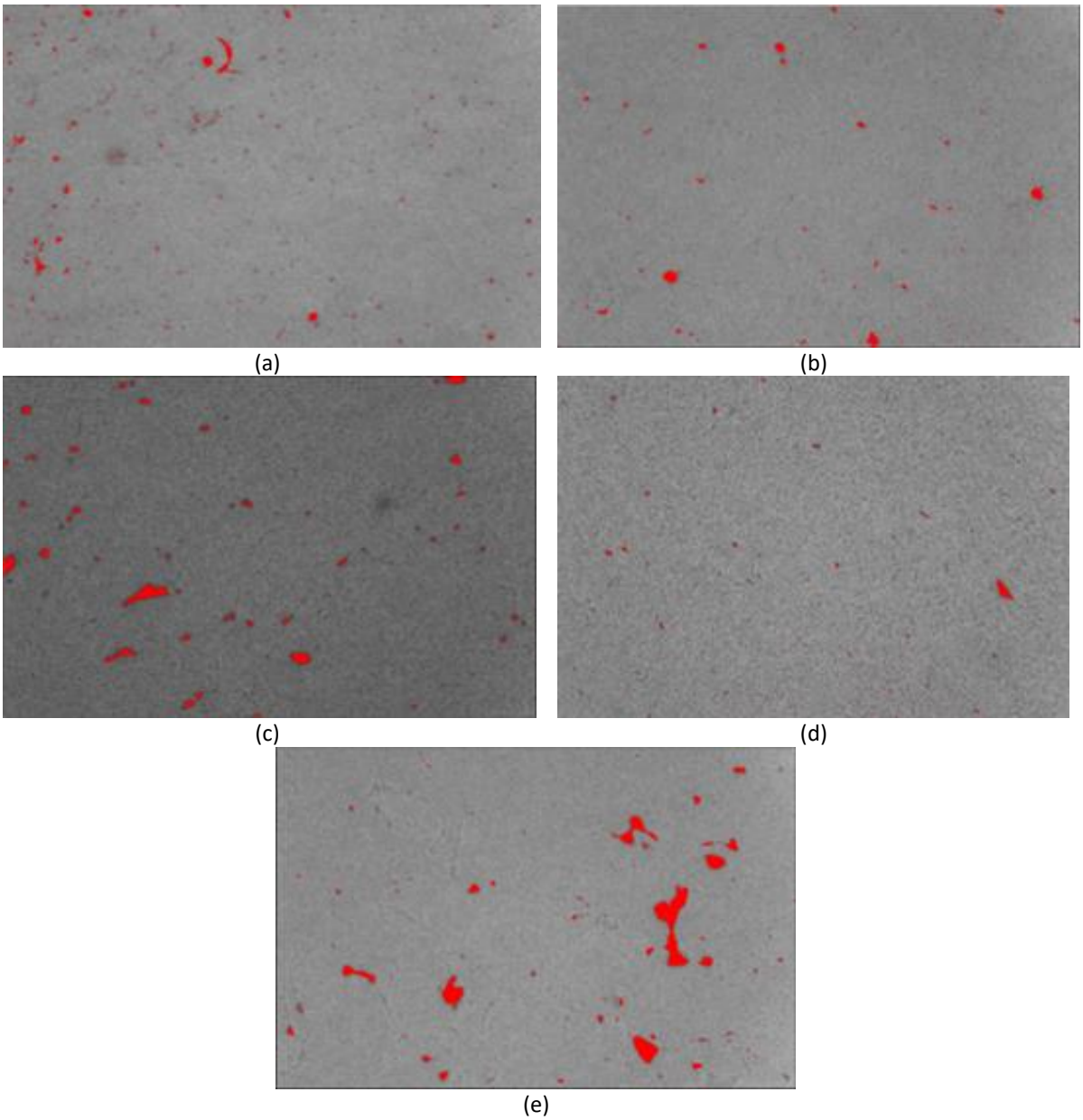

(a) (b) (c) (d) (e)

Figure 11: Porosity analysis through ImageJ software for each sample: (a) as-printed; (b) sample 1; (c) sample 2; (d) sample 3, and € sample 4.

3.4. Tensile Tests

The tensile tests results, that were performed in the specimens with HT-T6 (i) after printing and the ones as-printed, both in the perpendicular and in the parallel direction to the built plate, are shown in Table 7.

Samples	Thickness (mm)	Width (mm)	Yield stress (MPa)	Ultimate tensile strength (MPa)	Total elongation (%)
A1	3,448	4,480	234,6	339,9	17,99
A2	3,013	4,491	235,6	337,6	19,66
B1	3,489	4,486	243,3	290,9	3,03
B2	3,668	4,487	247,2	297,1	3,55
C1	3,53	4,508	112,5	191,7	18,96
C2	3,526	4,483	116,1	193,1	18,03
D1	3,507	4,512	117,9	201,7	22,00
D2	3,515	4,487	117,9	209,4	17,4

Table 7: Tensile test results for each condition tested.

Firstly, comparing the specimens that were submitted to HT-T6 (i) (A1, A2, B1 and B2), with the ones that were not (C1, C2, D1 and D2) represented also in the chart in Figure 12, it is possible to say that the first samples mentioned, have a higher value of yield strength than the second ones. This means that, when measured in the same direction, in both cases, the heat treatment improves the yield strength of this material.

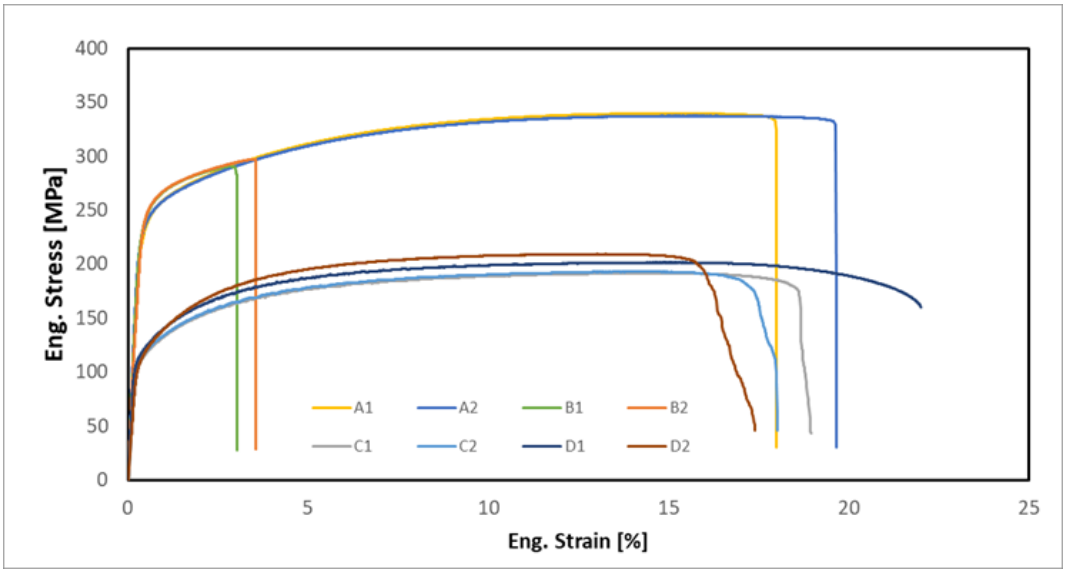

Figure 12: Chart representing Eng. Strain x Eng. Stress curves for each condition tested.

The same can be stated for the values obtained of ultimate tensile strength (UTS) results. This can be explained by the fact that the heat treatment provides the formation of spherical particles of eutectic Si and Fe-rich intermetallic compounds, which have a high hardness, increasing the UTS of this material, in both directions. Figure 13 represents the fracture surfaces of each sample, after the tensile tests.

Between the heat-treated samples (A and B), the ones tested in the perpendicular direction (A1 and A2) have a higher value of this property than the ones tested in the parallel direction (B1 and B2), since the cracks will propagate preferentially through the deposited layers of material as shown in Figure 13b. Nonetheless, the same does not apply to the non-heat-treated samples (C and D – Figure 13c and Figure 13d), even though that the difference between them is not meaningful (≈10 MPa).

Concerning the total elongation, it is possible to say that the HT samples that were tested in the same direction as the metal deposition (B), presents a brittle behavior, since the heat treatment provides an increase in the hardness of the material, through the formation of Fe-rich compounds and growth of Si precipitates, and furthermore, it is also promoted a preferential cracking through the layers. It is also possible to deduce that the samples are anisotropic since the tensile properties are not the same in both directions, being this more evident when the component is subjected to HT.

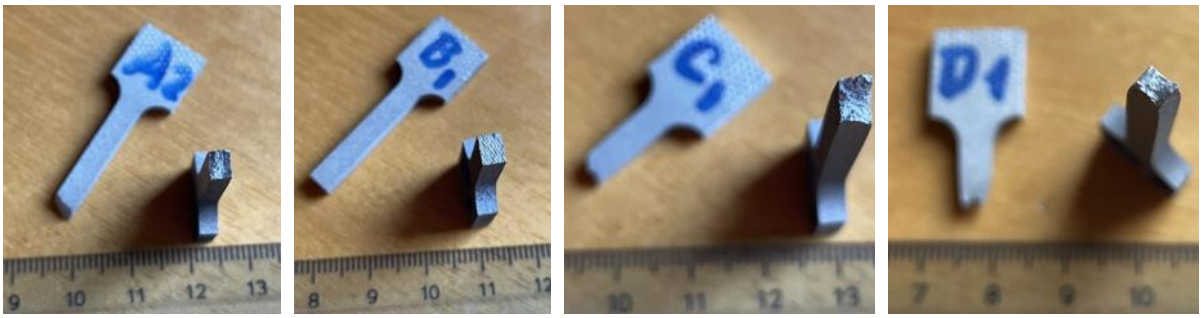

(a) (b) (c) (d)

Figure 13: Fracture surface resulting from each sample.

It can then be concluded that, if this material were to be put into service, it should be used in a perpendicular direction to the metal deposition, with heat treatment (in this case represented by sample A - Figure 13a), since this combination offers the highest elongation combined with the highest UTS.

Notice that the variation in the delay between quench and age, in the HT samples, keeping all the other parameters unchanged, might induce changes in the results of the mechanical properties studied. To demonstrate this, more tests would be needed.

4. Conclusions

The main goal of this practical work was to analyze and understand the influence of the HT conditions in the microstructural and mechanical properties of aluminum parts produced by liquid metal printing. The microstructural analysis was made on the perpendicular surface to the deposition direction, as well as the hardness tests and density analysis. Regarding to the tensile tests, the samples were pulled in both directions (perpendicular and parallel to the deposition direction). The microstructural characterization revealed the coalescence of particles of Si (AlSi2) and the precipitation of Fe- rich intermetallic compounds (β-Al5FeSi). About the hardness tests, it was verified that the HT promoted the increase of the hardness of the samples, however the difference between the two aging condition treatment do not induce a significative variation of this property. Concerning the density analysis, it was noted that the HT promotes a slight decrease in the porosity of the samples. Finally, the tensile tests had demonstrated that the samples pulled in the same direction as the deposition one, and heat treated, have a brittle behavior in comparison to the as-printed sample. Furthermore, it was noted, as expected that the HT induces an increase of the yield strength as well as the UTS.

To use these parts in service, it is recommended that they are used after being heat treated, in addition to being employed in the perpendicular direction to the deposition one, since this condition shows the best properties in tensile efforts.

References

American Institute of, Aeronautics, and Astronautics. "7.5 Processes and Materials". In *52nd AIAA/SAE/ASEE Joint Propulsion Conference, Salt Lake City, UT, July 25-27, 2016*: American Institute of Aeronautics and Astronautics (AIAA). https://app.knovel.com/hotlink/pdf/id:kt011K1MHN/52nd-aiaa-sae-asee-joint/processes-materials.

Ansell, Troy Y. 2021. "Current Status of Liquid Metal Printing". *Journal of Manufacturing and Materials Processing* 5, no. 2: 31. https://doi.org/10.3390/jmmp5020031.

Biswas, Prosanta, Surajit Patra, and Manas Mondal. 2020. "Structure-property correlation of eutectic Al-12.4 Si alloys with and without Zirconium (Zr) addition". *International Journal of Cast Metals Research* 33: 1-12. https://doi.org/10.1080/13640461.2020.1769319.

Chao, Wei, Liu Guang-lei, Wan Hao, Li Yu-shan, and Si Nai-chao. 2018. "Effect of Heat Treatment on Microstructure and Thermal Fatigue Properties of Al-Si-Cu-Mg Alloys". *High Temperature Materials and Processes* 37, no. 4: 289-98. https://doi.org/10.1515/htmp-2016-0199.

Chen, J., B. Shih, I. Adibnazari, Y. L. Park, and M. Tolley. 2022. "Open-loop printing of liquid metal for the low-cost rapid fabrication of soft sensors". Paper presented in 2022 IEEE 5th International Conference on Soft Robotics (RoboSoft), 4-8 April 2022. https://doi.org/10.1109/RoboSoft54090.2022.9762128

Corporation, United States Welding. "4008 (A356)". Accessed 26th of December of 2022. https://www.usweldingcorp.net/TDS/tds4181.pdf.

Domfang Ngnekou, Julius N., Yves Nadot, Gilbert Henaff, Julien Nicolai, and Lionel Ridosz. 2017. "Influence of defect size on the fatigue resistance of AlSi10Mg alloy elaborated by selective laser melting (SLM)". *Procedia Structural Integrity* 7: 75-83. https://doi.org/10.1016/j.prostr.2017.11.063.

Flow-3D. 2022. "Liquid Metal 3D Printing". Accessed 28th of December of 2022. https://www.flow3d.com/liquid-metal-3d-printing/.

Gülcan, Orhan, Kadir Günaydın, and Aykut Tamer. 2021. "The State of the Art of Material Jetting—A Critical Review". *Polymers* 13, no. 16: 2829. https://doi.org/10.3390/polym13162829.

Huang, Chi-Hsin, Yalun Tang, Tzu-Yi Yang, Yu-Lun Chueh, and Kenji Nomura. 2021. "Atomically Thin Tin Monoxide-Based p-Channel Thin-Film Transistor and a Low-Power Complementary Inverter". *ACS Applied Materials & Interfaces* 13, no. 44: 52783-92. https://doi.org/10.1021/acsami.1c15990.

ISO/ASTM. 2015. *ISO/ASTM 52900:2015(E), Additive manufacturing — General principles — Terminology*.

Kamara, Sheku, and Kathy S. Faggiani. "4.3.3 Metals". In *Fundamentals of Additive Manufacturing for the Practitioner - Additive Manufacturing Skills in Practice Series*: John Wiley & Sons. https://app.knovel.com/hotlink/pdf/id:kt012XDZV2/fundamentals-additive/metals.

Li, Qian, Ju Lin, Tian-Ying Liu, Xi-Yu Zhu, Wen-Hao Yao, and Jing Liu. 2021. "Gas-mediated liquid metal printing toward large-scale 2D semiconductors and ultraviolet photodetector". *npj 2D Materials and Applications* 5, no. 1: 36. https://doi.org/10.1038/s41699-021-00219-y.

Lumley, Roger N. *Fundamentals of Aluminium Metallurgy - Recent Advances*. Elsevier. https://app.knovel.com/hotlink/toc/id:kpFAMRA005/fundamentals-aluminium/fundamentals-aluminium.

Melamed, Yarden, Nabasmita Maity, Louisa Meshi, and Noam Eliaz. 2021. "Electroplating of Pure Aluminum from [HMIm][TFSI]–AlCl3 Room-Temperature Ionic Liquid". *Coatings* 11, no. 11: 1414. https://doi.org/10.3390/coatings11111414.

Reddy, P Ravinder, and P Anjani Devi. 2018. "Review on the advancements of additive manufacturing-4D and 5D printing". *Int J Mech Prod Eng Res Dev* 8, no. 4: 397-402.

Xerox. 2021. "Xerox® ElemX™ 3D Printer - System Specifications". Accessed 23/12/2022. https://www.xerox.com/downloads/usa/en/3d-printing/xerox-elemx-3dprinter-system-specifications-ENUS.pdf.

Acknowledgments

The authors would like to thank XEROX for providing samples which enabled this study.